Research Square

Preprints are preliminary reports that have not undergone peer review.
They should not be considered conclusive, used to inform clinical practice,
or referenced by the media as validated information.

Optimization of Cobalt Loading and Electrode Formulation in Carbon-Coated Si@Co Composite Anodes for Lithium-Ion Batteries

Siyu Wang
Shenyang Ligong University
Lijie Liu
liulijie@sylu.edu.cn

Shenyang Ligong University
Hongruo Kang
Shenyang Ligong University
Haitao Zhao
Shenyang Ligong University

Research Article

Keywords: Silicon anode, cobalt deposition, carbon coating, lithium-ion batteries, electrochemical performance

Posted Date: November 3rd, 2026

DOI: https://doi.org/10.21203/rs.3.rs-10554490/v1

License: This work is licensed under a Creative Commons Attribution 4.0 International License.
Read Full License

Additional Declarations: No competing interests reported.

Abstract

Silicon is a promising anode material for high-energy-density lithium-ion batteries, but its practical use is hindered by poor electrical conductivity, large volume changes, and progressive structural and interfacial degradation. This study investigated whether Co deposition and carbon coating could improve the electrochemical behavior of nanosilicon and identify suitable Co loading and electrode composition.HF-treated nanosilicon was decorated with different nominal amounts of Co through $NaBH_4$ reduction and subsequently coated with sucrose-derived carbon to obtain Si@Co/C composites. Their phase composition, morphology, and elemental distribution were characterized by X-ray diffraction, scanning electron microscopy, and energy-dispersive X-ray spectroscopy. Lithium-storage behavior and interfacial kinetics were evaluated using electrochemical measurements.

The crystalline Si framework was retained after Co incorporation. Microscopic and elemental analyses revealed the morphology of the composites and the distribution of Si, Co, and C. The composite containing 5 wt% Co, tested with an active material/Super P/PVDF mass ratio of 6:3:1, achieved the highest initial discharge capacity of approximately 1600 mAh g^{-1} and showed favorable capacity recovery during rate testing. Its Coulombic efficiency stabilized above 99.5% after the initial cycles. Nevertheless, the reversible capacity decreased to approximately 200 mAh g^{-1} after 400 cycles, indicating substantial long-term structural degradation. Moderate Co loading and optimization of the electrode formulation improved the initial capacity and reaction kinetics of Si-based composite anodes. Further stabilization of the electrode structure and interfaces is required to achieve durable cycling performance.

1 Introduction

The global transition toward low-carbon energy systems has intensified the demand for high-performance electrochemical energy storage. Owing to their high energy density and long cycle life, lithium-ion batteries (LIBs) are widely used in electric vehicles and grid-scale energy-storage systems [1–3] and have become a key technology supporting the transformation of modern energy infrastructure [4–5]. At the same time, electric vehicles require longer driving ranges, faster charging, and improved safety; portable electronics continue to evolve toward thinner and more powerful designs [6]; and stationary storage systems require batteries with both higher energy density and longer service life.

Silicon is an attractive anode material because of its high lithium-storage capacity [7]. Its theoretical specific capacity can reach 4200 mAh g^{-1} [8], approximately 11 times that of graphite, and its relatively low lithiation potential is favorable for high-energy-density LIBs [9–10]. These advantages are offset by a volume change of up to approximately 300% during lithiation and delithiation. Repeated expansion and contraction can pulverize Si particles, disrupt their electrical contact with the conductive network, and continuously rupture and reform the solid electrolyte interphase (SEI), leading to rapid capacity decay. In addition, Si is intrinsically semiconducting, with an electronic conductivity of approximately 10^{-5}-10^{-3} S cm^{-1} and a room-temperature Li-ion diffusion coefficient of only 10^{-14}-10^{-12} cm^2 s^{-1}, which limits its rate

capability [11]. The high surface reactivity of nanoscale Si can also promote electrolyte side reactions and the formation of a heterogeneous, unstable SEI, further compromising cycling stability and safety [12].

Several approaches have therefore been explored to improve the mechanical and electrical integrity of Si-based electrodes. Introducing a conductive secondary phase can maintain electron-transport pathways and help accommodate the stress generated by repeated volume changes [13–15]. Micro- and nanostructured Si/C composites provide a complementary strategy by shortening ion-transport distances and preserving electrical contact between Si and the carbon matrix during cycling [16]. Together, these findings suggest that coordinated control of the conductive phase, carbon framework, and electrode formulation is essential for balancing capacity and structural stability.

Cobalt (Co) is an electrically conductive and catalytically active transition metal that can facilitate interfacial charge transfer when incorporated into electrode architectures [17]. Carbon matrices, meanwhile, can improve electrical connectivity and provide free volume to accommodate the expansion of Si particles [18–19]. Combining Co with a carbon-coated Si framework is therefore expected to create additional conductive pathways, strengthen interparticle contact, and regulate the electrode/electrolyte interface. Related Co-containing carbon composites have also demonstrated the potential of such hybrid architectures for improving electrochemical reaction kinetics [20–21].

In this study, Si@Co/C composite anodes were synthesized by depositing Co onto nanosilicon through chemical reduction, followed by carbon coating using sucrose as the carbon precursor. The Co loading and active material/Super P/PVDF ratio were varied to determine their effects on phase composition, particle morphology, charge-transfer behavior, rate capability, and long-term cycling performance. The objective was to identify a practical combination of material composition and electrode formulation that improves electronic transport while mitigating the structural instability of Si.

2 Experimental

2.1 Surface Pretreatment of Silicon Powder

The native oxide layer on the Si powder was removed by etching with dilute HF. Briefly, 3 g of nanosilicon powder was added to 30 mL of 10% HF solution and magnetically stirred at room temperature. The suspension was then centrifuged, and the recovered powder was washed repeatedly with deionized water until the supernatant reached neutral pH. The product was vacuum-dried for 6 h to obtain oxide-free, activated Si powder.

2.2 Deposition of Co Particles by Chemical Reduction

Co particles with different nominal loadings were deposited on the surface of the activated Si powder through chemical reduction, using $CoCl_2 \cdot 6H_2O$ as the Co precursor and $NaBH_4$ as the reducing agent. A series of Co loadings was prepared to determine the optimal Co content.

1. Precursor dispersion: A predetermined amount of activated Si powder and an appropriate amount of polyvinylpyrrolidone (PVP) were dispersed in ethylene glycol and ultrasonicated for 30 min to minimize particle agglomeration. The required amount of Co precursor was then added, and the suspension was magnetically stirred at room temperature for 2 h to promote adsorption of Co ions onto the Si surface.
2. Low-temperature reduction: The suspension was placed in an ice-water bath, and 10 mL of 0.5 M $NaBH_4$ solution was added dropwise under continuous stirring over 2 h. Maintaining a low temperature moderated the reduction rate, minimized splashing caused by vigorous gas evolution, and promoted more uniform deposition of Co particles.
3. Centrifugation and drying: After the reduction reaction, the solid product was collected by centrifugation at 8000 rpm for 5 min and washed three times with anhydrous ethanol to remove residual solvent and soluble by-products. The product was then vacuum-dried at 60°C for 12 h to obtain the Si@Co composite.

2.3 Carbon-Coating Treatment

Sucrose was used as the carbon precursor to form a carbon coating on the Si@Co composite through high-temperature carbonization in a tube furnace. The carbon layer was introduced to improve electrical connectivity and to help accommodate the volume changes of Si during cycling.

1. Solid-state mixing: One gram of the as-prepared Si@Co composite and an appropriate amount of sucrose were weighed and thoroughly ground in an agate mortar to obtain a homogeneous mixture.
2. High-temperature carbonization: The mixed powder was loaded into a porcelain boat and placed in a tube furnace under flowing Ar. The furnace was heated to 750°C at 5°C min^{-1} and held at that temperature for 2 h to carbonize the sucrose. The product was then allowed to cool naturally to room temperature under Ar, yielding the Si@Co/C composite.

2.4 Electrode Preparation

The as-synthesized Si@Co/C composite was used as the active material, Super P as the conductive additive, poly(vinylidene fluoride) (PVDF) as the binder, and N-methyl-2-pyrrolidone (NMP) as the solvent. Electrodes with different component ratios were prepared to evaluate the influence of the electrode formulation. The preparation procedure was as follows.

1. Binder solution preparation: A 7 wt% PVDF solution was prepared in NMP.
2. Electrode powder mixing: Active material/Super P/PVDF mass ratios of 7:2:1 and 6:3:1 were evaluated. The components were ground in an agate mortar for 30 min.
3. Slurry preparation: The powder was mixed with the required amounts of 7 wt% PVDF/NMP solution and additional NMP, then stirred at 400 rpm for 12 h to form a homogeneous slurry.
4. Electrode coating: Cu foil was used as the current collector. Before coating, the foil was wiped with dilute nitric acid to remove surface oxides and contaminants, rinsed with anhydrous ethanol, and air-

dried. The slurry was cast uniformly onto the pretreated Cu foil using a film applicator with a nominal wet-film thickness of 200 μm.
5. Vacuum drying: The coated electrodes were vacuum-dried at 80°C for 3 h and then at 110°C for 12 h before cell assembly.

2.5 Cell Assembly

CR2032 coin cells were assembled in an Ar-filled glovebox using Si@Co/C as the working electrode, Li metal as the counter/reference electrode, a Celgard 2500 separator, and $LiPF_6$ electrolyte in EC/DEC/DMC (1:1:1).

1. Active-material mass determination: The active-material mass in each electrode was determined by differential weighing. The mass of the dried coated electrode (m_1) and that of a blank Cu-foil disk of the same size (m_2) were recorded. The active-material mass was calculated as $m_{AM} = (m_1 - m_2) \times w_{AM}$, where w_{AM} is the active-material mass fraction in the coating. The active material/conductive additive/binder ratio was expressed as *x*:(90 - *x*):10, with *x* = 60, 70, or 80.
2. Lithium-foil preparation: Surface oxides were gently scraped from both sides of the Li foil before assembly.
3. Cell assembly and aging: The working electrode and separator were wetted with electrolyte, followed by sequential stacking of the Li foil, stainless-steel spacer, wave spring, and opposite case. The cells were crimped and aged at room temperature for 12 h before testing.

2.6 Material Characterization and Electrochemical Measurements

The morphology of the as-prepared materials was examined using a TESCAN VEGA3 scanning electron microscope (SEM) equipped with an energy-dispersive X-ray spectrometer (EDS); elemental point analyses and mapping were used to evaluate the elemental distribution. X-ray diffraction (XRD) patterns were collected using a Shimadzu Ultima IV diffractometer with Cu Kα radiation (λ = 1.5418 Å) at 40 kV and 40 mA. Data were acquired over a 2θ range of 10°-80° with a step size of 0.02°. EIS, CV, rate capability, and galvanostatic cycling were measured using a 4192A low-frequency impedance analyzer, a Pine Research AFP2 workstation, and a CT-ZWJ-4S-T-1U battery-testing system.

3 Results and Discussion

3.1 Phase and Morphological Characterization

As shown in Fig. 2, both samples exhibit the characteristic reflections of crystalline Si at approximately 2θ = 28.4°, 47.3°, and 56.1°, with no discernible shift in peak position. This result indicates that the Si lattice was retained after Co deposition and that Co was not measurably incorporated into the Si lattice. The 7 wt% Co sample shows more intense Si reflections and more evident Co-related features than the 5

wt% Co sample, suggesting a difference in crystallinity and Co content between the two composites. These results confirm the coexistence of crystalline Si and the deposited Co-containing phase.

Figure 3 compares the Si@Co/C composite electrode before and after cycling. Before cycling (Fig. 3a and b), the particles are relatively uniformly distributed, with interparticle voids that facilitate electrolyte penetration and Li-ion transport. The electrode surface is smooth and free of obvious cracks, agglomeration, or delamination. After cycling (Fig. 3c and d), pronounced particle fragmentation, structural collapse, and electrode cracking are observed. These changes are attributed to the repeated volume expansion and contraction of Si, which exceed the buffering capacity of the carbon coating and progressively disrupt the electrode structure.

As shown in Fig. 4a and b, the sample prepared without PVP exhibits pronounced particle agglomeration and irregular stacking, resulting in dense secondary aggregates. The limited interparticle porosity provides insufficient space to accommodate Si expansion and may also impede electrolyte penetration and ion transport.

In comparison, the PVP-assisted sample (Fig. 4c and d) displays a more open morphology and improved particle dispersion. The Si particles are distributed within the carbon matrix and covered by carbonaceous material, forming a porous three-dimensional network. This architecture is expected to improve electrical connectivity and ion transport while providing additional space to accommodate the volume changes of Si.

The SEM and EDS results in Fig. 5 show that the composite is composed mainly of secondary particles assembled from nanoscale primary particles, without extensive macroscopic agglomeration. This morphology indicates that the synthesis procedure limits the coalescence of the primary particles and may reduce localized stress concentration during cycling.

Elemental mapping shows that Si, Co, and C are distributed throughout the analyzed region, indicating that the deposited Co and carbonaceous components are in close contact with the Si particles. Such spatial integration is favorable for forming continuous electron-transport pathways and for distributing the stress associated with Si volume changes. The EDS results further confirm the successful incorporation of Co into the composite. Overall, the combined SEM and EDS observations support the formation of a multicomponent Si@Co/C architecture with relatively uniform elemental distribution.

3.2 Electrochemical Performance

The electrochemical performance of the Si@Co/C electrodes was evaluated as a function of Co loading and electrode formulation. As shown in Fig. 6a, all samples exhibit the characteristic voltage profiles of Si-based anodes. The electrodes containing 5 wt% Co deliver higher capacities than those containing 10 wt% Co. In particular, the 5 wt% Co electrode with an active material/Super P/PVDF mass ratio of 6:3:1 achieves the highest initial discharge capacity, approximately 1600 mAh g^{-1}.

Figure 6b and c show the first three charge-discharge profiles of the electrodes containing 5 wt% Co at different component ratios. The pronounced irreversible capacity loss in the first cycle is primarily associated with SEI formation, electrolyte decomposition, and partially irreversible lithiation. The second and third profiles overlap much more closely, indicating improved lithiation/delithiation reversibility after the initial activation cycle. The 6:3:1 electrode delivers a higher reversible capacity than the 7:2:1 electrode, demonstrating the importance of sufficient conductive additive for utilizing the active material.

As shown in Fig. 6d, the specific capacity decreases as the current density increases because of enhanced polarization and increasingly limited Li-ion transport. When the current density is returned to 0.1 A g^{-1}, the capacity recovers substantially, indicating that much of the rate-induced capacity loss is reversible. The Coulombic efficiency rises rapidly during the initial cycles and subsequently approaches 100%, consistent with progressively stabilized interfacial reactions.

The CV curves are shown in Fig. 6e and f. During the first cathodic scan, the reduction feature at approximately 0.7 V is assigned to electrolyte decomposition and SEI formation; its disappearance in subsequent scans indicates that these reactions occur predominantly during the first cycle. The strong cathodic response below 0.2 V corresponds to Si lithiation, whereas the anodic peak near 0.5 V is associated with Si delithiation. The close overlap of the second and third cycles indicates improved reversibility after activation. Relative to the 7:2:1 electrode, the 6:3:1 electrode exhibits higher peak currents and more distinct redox features, consistent with more favorable reaction kinetics and the galvanostatic results.

As shown in Fig. 7a, the electrodes containing 5 wt% Co deliver an initial discharge capacity of approximately 1600 mAh g^{-1}. The capacity decreases rapidly during the early cycles and then stabilizes at approximately 200 mAh g^{-1} after 400 cycles. At the same Co loading, the two electrode formulations exhibit similar long-term capacities, indicating that the slurry ratio has only a limited effect on the stabilized capacity under the present conditions. Thus, although the Co/carbon architecture and optimized formulation improve the initial utilization of Si, they do not completely suppress the structural and interfacial degradation that occurs during prolonged cycling.

The EIS results are presented in Fig. 7b. The similar high-frequency intercepts indicate relatively low solution and contact resistances for all four electrodes. At a given Co loading, the electrodes with a 6:3:1 component ratio exhibit smaller semicircles than the corresponding 7:2:1 electrodes. Moreover, the 5 wt% Co electrodes show smaller mid-frequency semicircles than the 10 wt% Co electrodes at the same component ratio, indicating lower charge-transfer resistance (R_{ct}). Excessive Co deposition may hinder interfacial Li-ion transport despite increasing the amount of conductive metal. In the low-frequency region, the 5 wt% Co (6:3:1) electrode exhibits the steepest inclined tail, consistent with the lowest diffusion impedance among the tested electrodes, whereas the 10 wt% Co (7:2:1) electrode shows the shallowest slope.

Taken together, the EIS results identify the electrode containing 5 wt% Co with a 6:3:1 component ratio as having the most favorable overall interfacial kinetics. This interpretation is consistent with its charge-

discharge behavior and rate capability.

4 Conclusions

Si@Co/C composite anodes were prepared by chemical reduction and subsequent carbon coating to address the low electrical conductivity, large volume changes, and interfacial instability of Si. The effects of Co loading and electrode formulation on the phase composition, microstructure, and electrochemical behavior were systematically evaluated.

(1) Phase and morphology. The characteristic reflections of crystalline Si were retained in the composites containing 5 and 7 wt% Co, with no measurable shift in the Si peak positions. The 7 wt% Co sample exhibited more intense diffraction features. PVP-assisted synthesis produced a more open particle architecture than the PVP-free route, while SEM/EDS analysis confirmed close spatial integration and relatively uniform distribution of Si, Co, and C. Nevertheless, marked particle fragmentation and electrode cracking were observed after cycling, demonstrating that the composite architecture did not fully accommodate the repeated volume changes of Si.

(2) Electrochemical behavior. The electrode containing 5 wt% Co with an active material/Super P/PVDF ratio of 6:3:1 delivered the highest initial discharge capacity of approximately 1600 mAh g^{-1} and showed favorable capacity recovery during rate testing. Its CV response indicated improved reversibility after the first activation cycle, and its EIS spectrum was consistent with comparatively favorable charge-transfer and diffusion kinetics. During long-term cycling, however, the capacity stabilized at approximately 200 mAh g^{-1} after 400 cycles, highlighting the need for further optimization of the mechanically resilient conductive framework and interphase.

Overall, moderate Co loading and optimization of the electrode formulation improved the initial lithium-storage response and interfacial kinetics of the Si@Co/C composite. The remaining long-term capacity decay shows that future work should focus on strengthening the carbon framework, controlling Co distribution, and stabilizing the SEI. These findings provide a useful basis for the rational design of multicomponent Si-based anodes.

Declarations

Author Contribution

Siyu Wang and Lijie Liu wrote the main manuscript text, Siyu Wang prepared figures 1-5, Hongruo Kang prepared figures 6-7, and Haitao Zhao revised the manuscript text. All authors reviewed the manuscript.

Acknowledgements

The authors would like to acknowledge the funding support from the Joint Funds of Natural Science Foundation of Liaoning Province (2025-MSLH-591).

References

1. Mahmood AS, Mobarak NN, Khudayberdieva A et al (2025) Silicon Carbide (SiC) and Silicon/Carbon (Si/C) Composites for High-Performance Rechargeable Metal-Ion Batteries[J]. Int J Mol Sci 26(16):7757
2. Jin B, Liao L, Shen X et al (2025) Advancement in Research on Silicon/Carbon Composite Anode Materials for Lithium-Ion Batteries[J]. Metals 15(4):386
3. Chen J, Wang X, Deng Z et al (2025) Facile synthesis of Si/C composites for high-performance lithium-ion battery anodes.[J]. Nanoscale 17:6049–6057
4. Park I, Lee H, Chae BO (2024) Synthesis Methods of Si/C Composite Materials for Lithium-Ion Batteries[J]. Batteries 10(11):381
5. Yang L, Li S, Zhang Y et al (2024) Multi-scale design of silicon/carbon composite anode materials for lithium-ion batteries:A review[J]. J Energy Chem 97:30–45
6. Tae-Hyun H, Hye-Rim BSR (2023) A study on the electrochemical properties of silicon/carbon composite for lithium-ion battery[J]. J Energy Storage 63:107045
7. Yu P, Li Z, Zhang D et al (2024) Hierarchical Yolk-Shell Silicon/Carbon Anode Materials Enhanced by Vertical Graphene Sheets for Commercial Lithium-Ion Battery Applications[J]. Adv Funct Mater 35(2):2413081–2413081
8. Ahmed H, Reis DSG, Molaiyan P et al (2025) Silicon/carbon composite anode materials for lithium-ion batteries:materials design and synthesis, current state, progress, and future perspectives[J]. Progress Energy 7(2):149–198
9. Yang B, Xin C, Zhanyuan T et al (2021) A high-performance silicon/carbon composite as anode material for lithium ion batteries[J]. Nano Express 2(1):10021
10. Wei X, Cheng N, Chengdong X et al (2022) Effect of silicon/carbon composite on properties of Graphite anode materials in Li-ion batteries[J]. Int J Electrochem Sci 17(11):221117
11. Jiao P, Li W, Zhenyu W et al (2022) Si/C composite embedded nano-Si in 3D porous carbon matrix and enwound by conductive CNTs as anode of lithium-ion batteries[J]. Sustainable Mater Technol 32:10
12. Yu H, Fei W et al (2021) Optimal microstructural design of pitch-derived soft carbon shell in yolk-shell silicon/carbon composite for superior lithium storage[J]. Electrochim Acta 373:137927
13. Niu J, Shen D, Ren Z et al (2026) The influence of carbon sources on the structural and electrochemical performance of silicon-carbon composite anodes for lithium-ion batteries[J]. J Mater Sci 61(5):1–15
14. Chen L, Ye Q, Han C et al (2025) Boron-doped SiOC anode material with an yolk shell multistage structure for lithium-ion batteries[J]. Int J Electrochem Sci 20(9):101099

15. Xing L (2023) Analysis of research progress in improving the performance of silicon-based anode materials for lithium-ion batteries: a combination of nanostructured silicon and silicon-based composites[J]. Journal of Physics: Conference Series, 2608(1):012001
16. Kwon HJ, Hwang JY, Shin HJ et al (2020) Nano/Microstructured Silicon-Carbon Hybrid Composite Particles Fabricated with Corn Starch Biowaste as Anode Materials for Li-Ion Batteries[J]. Nano Lett 20(1):625–635
17. Xin W, Wang Q, Yang D et al (2026) In-situ metallic cobalt layer for multifunctional synergistic effects in high-performance Lithium metal batteries[J]. Chem Eng J 532:174399
18. Ni C, Xia C, Liu W et al (2024) Effect of Graphene on the Performance of Silicon-Carbon Composite Anode Materials for Lithium-Ion Batteries. [J]. Materials (Basel, Switzerland), 17(3):754
19. Mingcai Z, Juan Z, Xiaoguang Z et al (2023) Application of high-strength, high-density, isotropic Si/C composites in commercial lithium-ion batteries[J]. Energy Storage Mater 61:102857
20. Hyun DK, Dae GP, Chan YK (2022) Electrochemical properties of yolk-shell structured cobalt hydroxy chloride-carbon composite as an anode for lithium-ion batteries[J]. Int J Energy Res 46(7):9761–9770
21. Jin-Sung P, Dae GP, Chan YK (2021) .Exploration of cobalt selenite-carbon composite porous nanofibers as anode for sodium-ion batteries and unveiling their conversion reaction mechanism[J]. J Mater Sci Technol 89:24–35

Figures

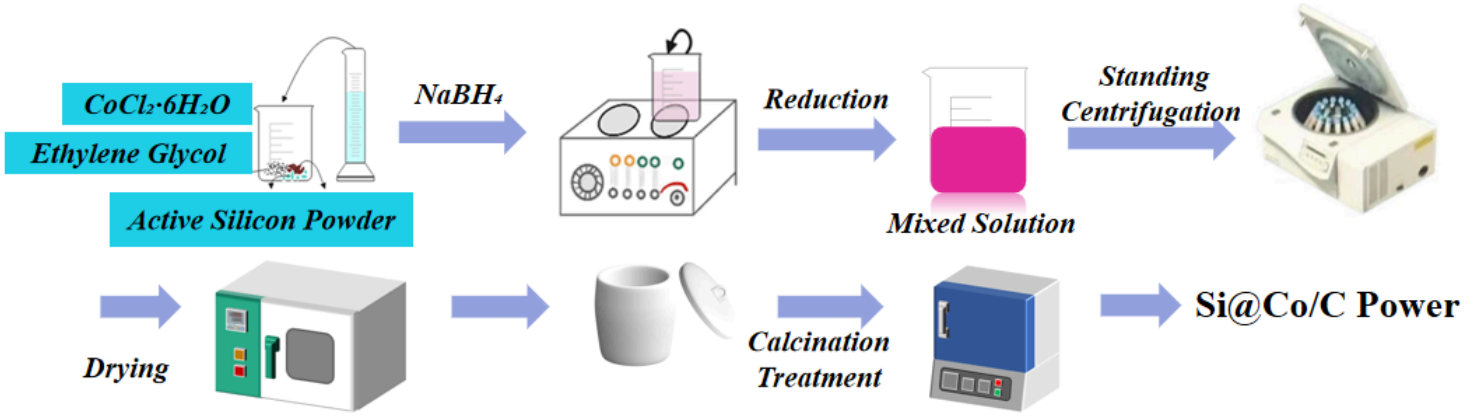


Figure 1

Schematic diagram of the experimental procedure

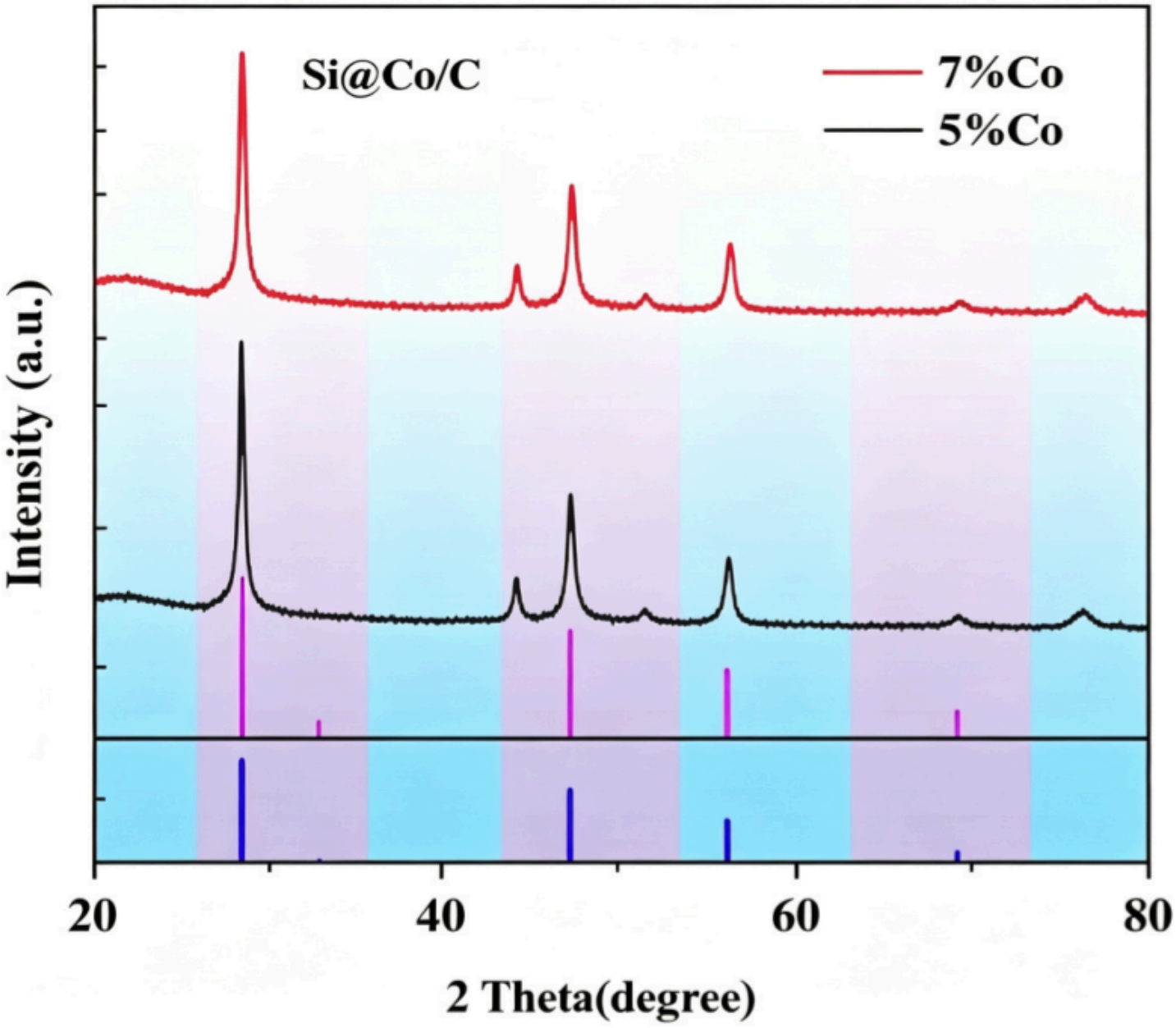


Figure 2

XRD patterns of Si@Co/C composites with Co loadings of 5 and 7 wt%.

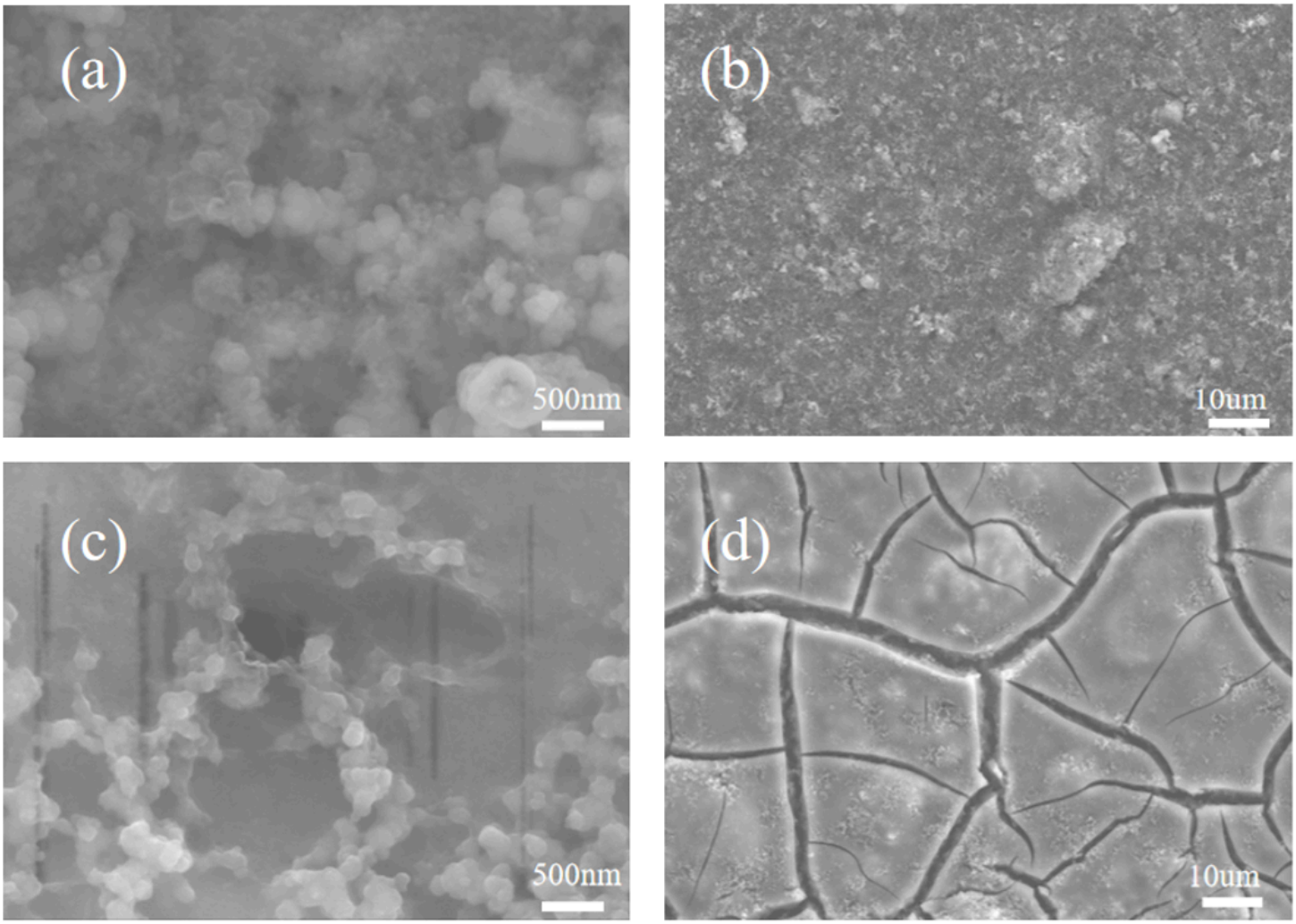


Figure 3

SEM images of the Si@Co/C composite electrode (a, b) before cycling and (c, d) after cycling.

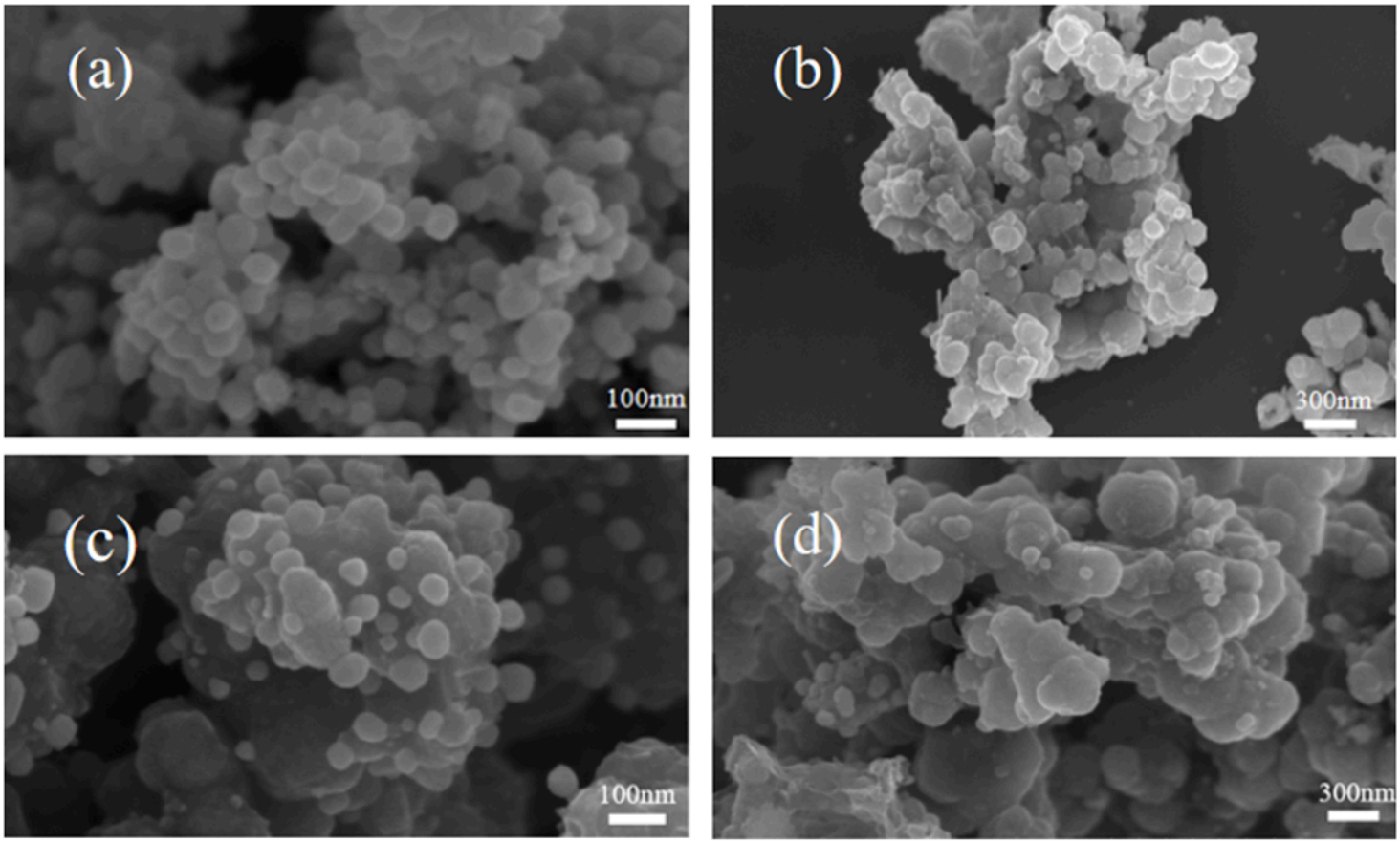
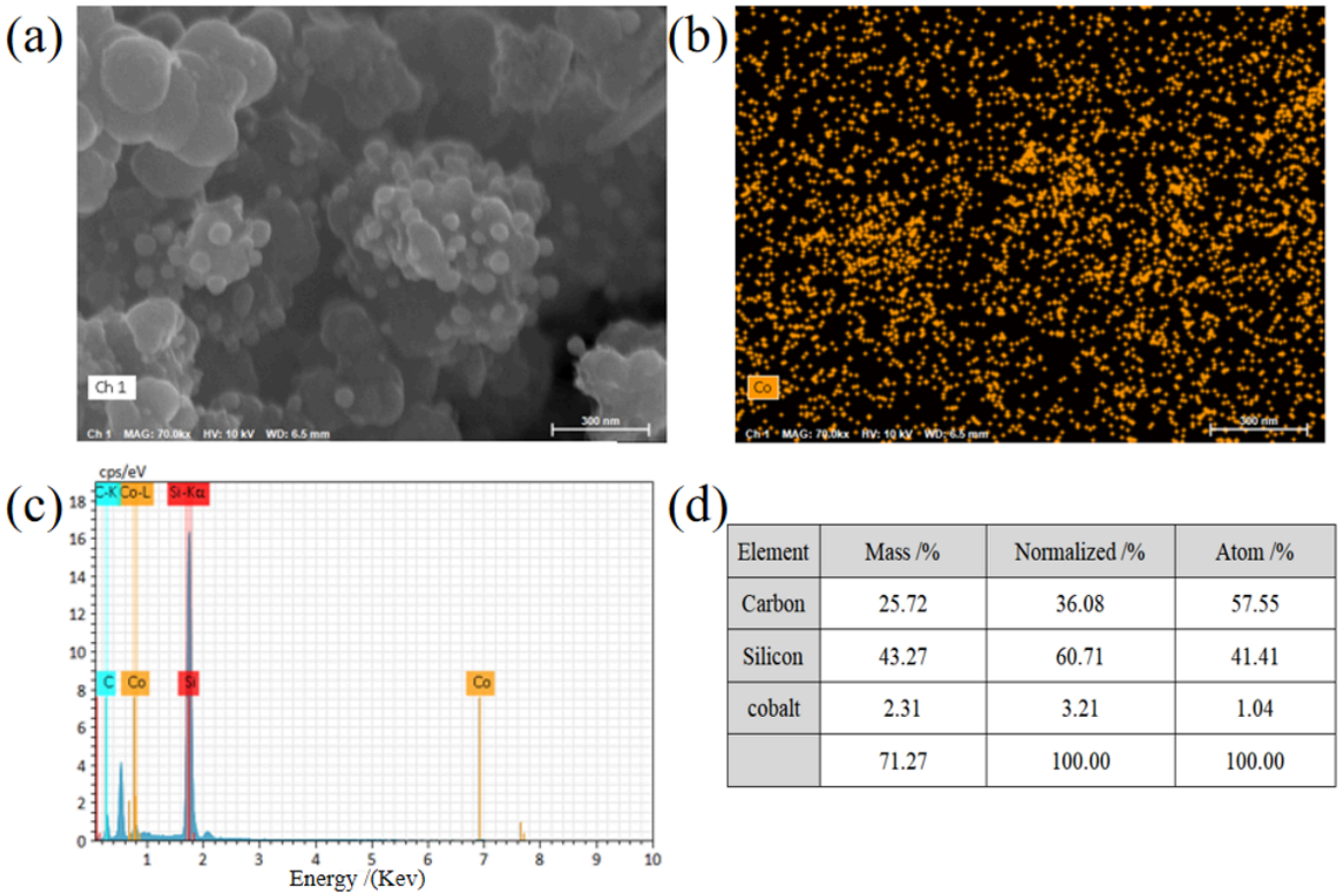


Figure 4

SEM images of Si@Co/C composites prepared (a, b) without PVP and (c, d) with PVP.



Element	Mass /%	Normalized /%	Atom /%
Carbon	25.72	36.08	57.55
Silicon	43.27	60.71	41.41
cobalt	2.31	3.21	1.04
	71.27	100.00	100.00

Figure 5

(a)–(b) SEM images and EDS point-scan results of the Si@Co/C composite electrode material; (c) corresponding EDS spectrum; (d) total spectrum of elemental mapping.

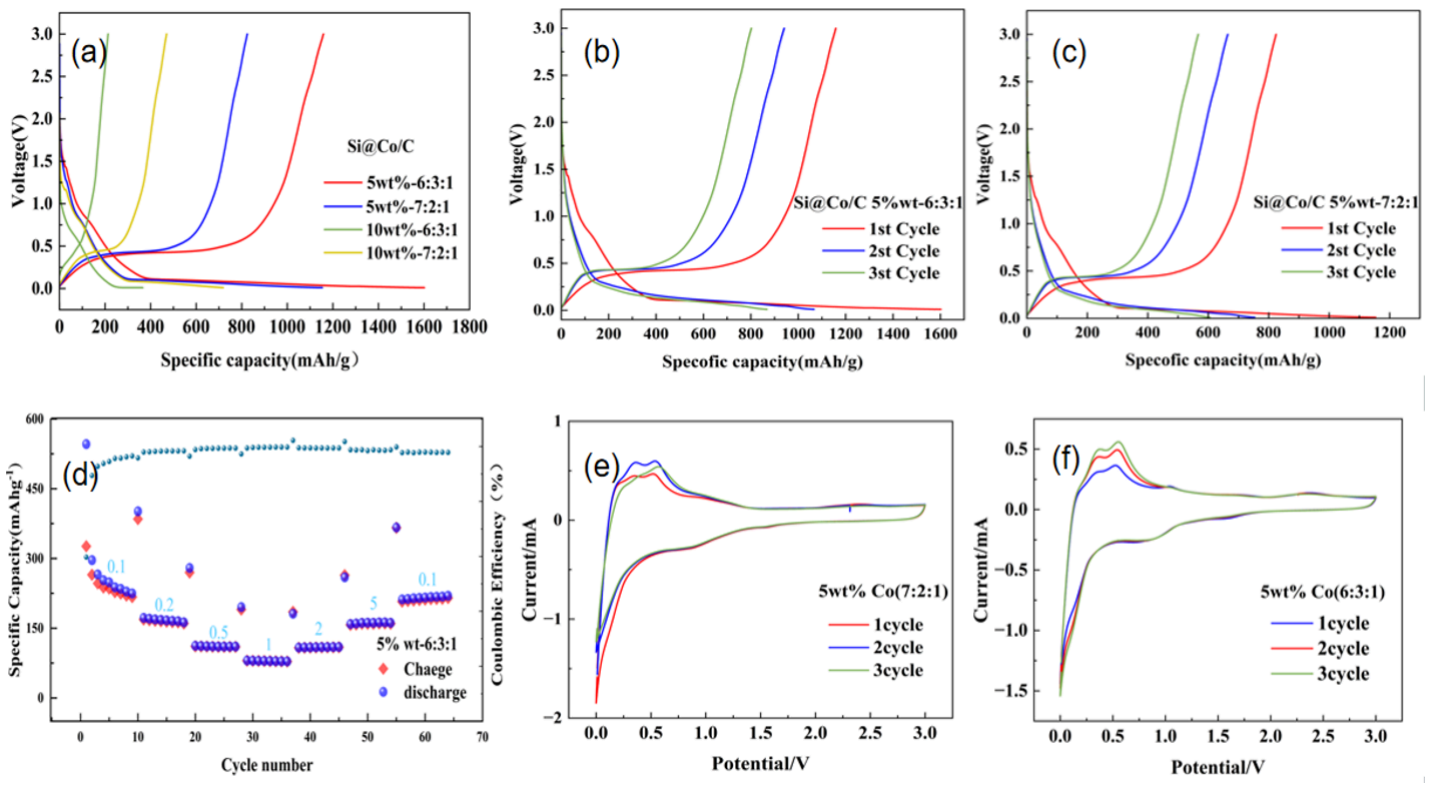


Figure 6

(a) Initial charge-discharge profiles of electrodes with different Co loadings and component ratios; (b, c) first three charge-discharge profiles of electrodes containing 5 wt% Co with active material/Super P/PVDF ratios of 6:3:1 and 7:2:1, respectively; (d) rate capability of the 5 wt% Co Si@Co/C electrode; and (e, f) CV curves of the 5 wt% Co electrodes with component ratios of 7:2:1 and 6:3:1, respectively.

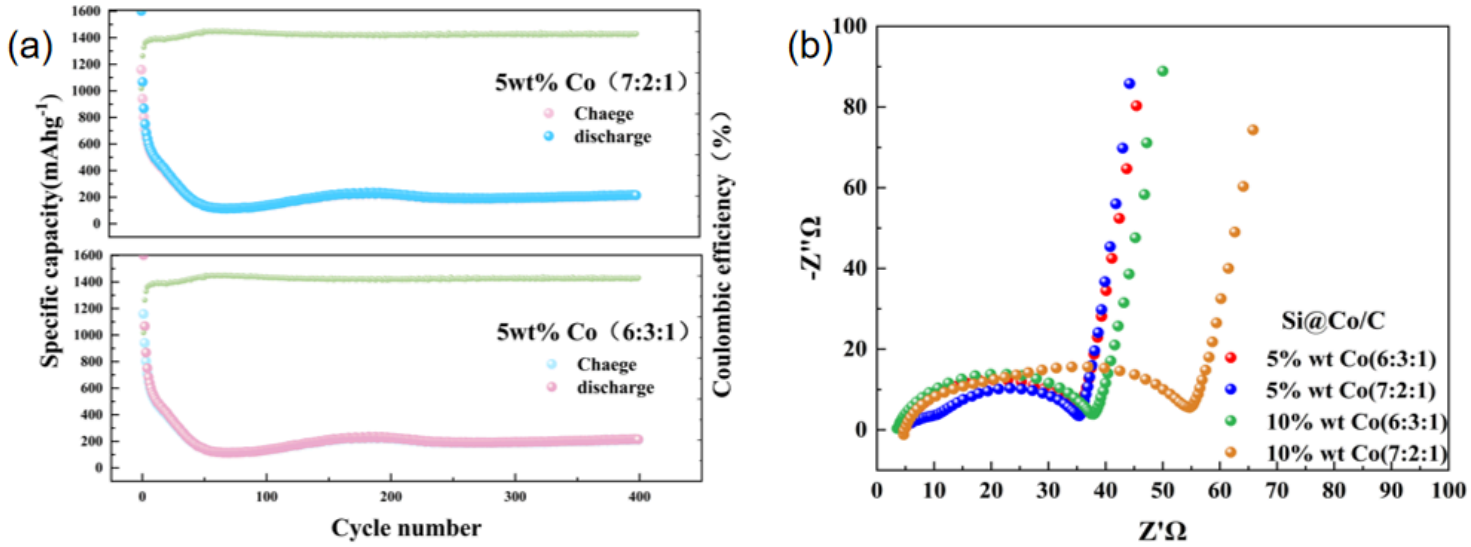


Figure 7

(a) Long-term cycling performance of Si@Co/C electrodes containing 5 wt% Co with active material/Super P/PVDF ratios of 7:2:1 and 6:3:1; (b) EIS spectra of Si@Co/C electrodes with different Co loadings and component ratios.